ADVANCED MATERIALS
www.advmat.de

A 2D/3D Heterostructure Perovskite Solar Cell with a Phase-Pure and Pristine 2D Layer

*Meng-Chen Shih, Shaun Tan, Yongli Lu, Tim Kodalle, Do-Kyoung Lee, Yifan Dong, Bryon W. Larson, Soyeon Park, Ruiqi Zhang, Matthias J. Grotevent, Tara Sverko, Hua Zhu, Yu-Kuan Lin, Carolin M. Sutter-Fella, Kai Zhu, Matthew C. Beard, Vladimir Bulović, and Moungi G. Bawendi**

Interface engineering plays a critical role in advancing the performance of perovskite solar cells. As such, 2D/3D perovskite heterostructures are of particular interest due to their optoelectrical properties and their further potential improvements. However, for conventional solution-processed 2D perovskites grown on an underlying 3D perovskite, the reaction stoichiometry is normally unbalanced with excess precursors. Moreover, the formed 2D perovskite is impure, leading to unfavorable energy band alignment at the interface. Here a simple method is presented that solves both issues simultaneously. The 2D formation reaction is taken first to completion, fully consuming excess PbI_2. Then, isopropanol is utilized to remove excess organic ligands, control the 2D perovskite thickness, and obtain a phase-pure, $n = 2$, 2D perovskite. The outcome is a pristine (without residual 2D precursors) and phase-pure 2D perovskite heterostructure with improved surface passivation and charge carrier extraction compared to the conventional solution process. PSCs incorporating this treatment demonstrate a notable improvement in both stability and power conversion efficiency, with negligible hysteresis, compared to the conventional process.

1. Introduction

Organic–inorganic lead halide perovskite solar cells (PSCs) have attracted widespread attention due to their low-cost fabrication, excellent photoelectric properties, and soaring power conversion efficiency (PCE).[1–5] Interface passivation has significantly contributed to the efficiency and stability improvements of PSCs. Among all the methods to modify the interface, constructing 2D/3D perovskite heterostructures has been the most widespread and has led to high-performance devices.[6–11] Most typically, the 2D layer is grown in a solution processing step by adding the 2D organic ligand on the 3D perovskite surface to trigger 2D perovskite formation.[2,12,13] Two main issues arise, however, during this conventional formation of the 2D layer. First, since it is challenging to quantify the reaction stoichiometry, the reaction is typically unbalanced, and

M.-C. Shih, S. Tan, Y. Lu, M. J. Grotevent, T. Sverko, H. Zhu, Y.-K. Lin, M. G. Bawendi
Department of Chemistry
Massachusetts Institute of Technology
77 Massachusetts Avenue, Cambridge, MA 02139, USA
E-mail: mgb@mit.edu

T. Kodalle, D.-K. Lee, C. M. Sutter-Fella
Molecular Foundry Division
Lawrence Berkeley National Laboratory
67 Cyclotron Road, Berkeley, CA 94720, USA

The ORCID identification number(s) for the author(s) of this article can be found under https://doi.org/10.1002/adma.202416672

DOI: 10.1002/adma.202416672

T. Kodalle
Advanced Light Source
Lawrence Berkeley National Laboratory
6 Cyclotron Road, Berkeley, CA 94720, USA

D.-K. Lee
Nevada Extreme Conditions Laboratory
University of Nevada
Las Vegas, NV 89154, USA

Y. Dong, B. W. Larson, S. Park, K. Zhu, M. C. Beard
Chemistry and Nanoscience Center
National Renewable Energy Laboratory (NREL)
15013 Denver West Parkway, Golden, CO 80401, USA

R. Zhang, V. Bulović
Department of Electrical Engineering and Computer Science
Massachusetts Institute of Technology (MIT)
77 Massachusetts Avenue, Cambridge, MA 02139, USA

excess organic ligands or excess PbI_2 often remain as reaction byproducts. Secondly, the reaction is rapid and uncontrollable, resulting in the formation of impure 2D phases with unfavorable energy alignments, hindering carrier extraction.[14,15]

Recently, there have been many attempts to resolve both issues, including different organic ligand designs,[16,17] precursor and chemical compositional engineering,[18,19] and fabrication process manipulation.[20,21] For example, vacuum deposition methods have been developed to grow 2D perovskites with a high-purity controlled 2D phase.[22–25] Solid-state in-plane growth methods have been shown to form a highly crystalline phase-pure 2D perovskite.[26] Dissolving the parent crystal powder in solution to grow 2D perovskites has also been shown to form 2D perovskites with the desired composition and 2D phase.[27] However, these methods generally require synthesizing the target 2D perovskite single crystal, or they require special deposition conditions like vacuum, which are more complex and expensive than conventional solution methods. More importantly, almost no solution-processed method exists that can concurrently solve both issues: an impure 2D phase and unbalanced stoichiometry.

We present here a simple solution-based method, that can achieve both goals simultaneously without the need for synthesizing a single crystal. Our method creates a phase-pure 2D perovskite without excess byproducts. In our method, we first push a complete 2D perovskite formation reaction. Next, a choice solvent, isopropanol (IPA), is selected to control the 2D perovskite thickness and remove the excess organic ligand. The final result is a phase-pure, $n = 2$, 2D perovskite layer with a favorable band alignment between the 3D perovskite and charge-transport layer. The high quality of this 2D perovskite layer is verified by studying its carrier dynamics, with a 250% increase in the surface diffusion coefficient and a 47% increase in carrier lifetime compared to a conventional 2D method. The target devices also demonstrate negligible hysteresis and significantly improved long-term stability and PCE compared to the conventional method, with the champion device reaching a PCE of 25.3%.

2. The Process of Our Method, Modification from the Conventional 2D Solution Method

In the typical solution-processed 2D perovskite growth, a reaction occurs between the PbI_2, the small "A" site organic cation (such as $CH_3NH_3^+$ (MA^+) or $[HC(NH_2)_2]^+$ (FA^+)), and the bulky organic ligand (such as $C_8H_{17}NH_3^+$ (OA^+) or $C_6H_{13}NH_3^+$ (HA^+)).[28] The chemical reaction can be described with the following Equation (1):

$$n\left(PbX_2\right) + (n-1)\,AX + 2\,(LX) \rightarrow L_2A_{n-1}Pb_nX_{3n+1} \quad (1 \le n < \infty) \quad (1)$$

where A, L, and X correspond to the "A" site organic cation, the bulky organic ligand, and the halide anion, respectively. Different n values refer to the formation of different 2D phases. In reaction (1), the PbI_2 comes from excess PbI_2 from the 3D perovskite growth process, and from the IPA dissolving part of the 3D perovskite surface. The AX originates from the dissolved 3D perovskite surface, while the LX is the organic ligand introduced to the 3D perovskite surface as shown in **Figure 1a**.[2,12,13]

Several major problems arise during the typical solution process as shown in the grazing-incident wide-angle X-Ray scattering (GIWAXS) graph in Figure 1b and are illustrated in the schematic of Figure 1c. First, achieving a balanced stoichiometry with no excess precursors during 2D perovskite formation is very challenging. More specifically, since we cannot quantify the exact amount of PbI_2 on the 3D perovskite surface, and we add the organic ligand as a post-processing step, it is impossible to quantify how much organic ligand is needed to achieve a complete reaction with no excess precursors. One of two possible scenarios will occur during the chemical reaction—either the PbI_2 or the organic ligand will be excess in the unbalanced reaction. If PbI_2 is in excess, which is the most common occurrence during conventional 2D formation as shown in Figure 1b,c, the unreacted PbI_2 will decompose to Pb^0 and I_2 under light illumination, reducing the stability of the PSC.[29,30] On the other hand, if the organic ligand is in excess, although the formed excess 2D perovskite can effectively passivate the surface resulting in an impressive carrier lifetime,[31] the residual organic ligand and an overly thick 2D perovskite layer lead to an insulating layer on top of the 3D perovskite as illustrated in Figure S1 (Supporting Information), significantly increasing the resistance of the PSC, reducing the fill factor (*FF*) and PCE of the device as shown in Figure S2 (Supporting Information).[31,32] The second major problem is the formation of mixed 2D phases due to the rapid and uncontrollable chemical reaction during solution-processing of the 2D perovskite. Both $n = 1$ and $n = 2$, 2D perovskite phases, form as shown in Figure 1b,c. Since different 2D phases have different bandgaps and band alignments, the impure 2D phase results in an inhomogeneous energy landscape and unfavorable band alignments, leading to more voltage loss during carrier transfer.[33]

Our new method to grow the 2D perovskite layer achieves a net balanced stoichiometry between the reactants. In addition, our approach results in a phase-pure 2D perovskite with no mixed 2D phases. Our method achieves both goals concurrently without the need for synthesizing a single crystal, whereas almost no other method exists in the literature that can attain both goals together. Figure 1d shows the procedure of the process. Firstly, we make the organic ligand the excess reagent, with PbI_2 the limiting reagent. Since we can control the amount of the organic ligand, while PbI_2 is just leftover on the 3D perovskite, we make the organic ligand the excess reagent by introducing it in a highly concentrated solution. From the reaction perspective, this means we force the PbI_2 in Equation (1) to completely react, forming the 2D perovskite. Nevertheless, as shown in Figures S1 and S2 (Supporting Information), the concentrated organic ligand solution leads to residual organic ligands and a thick 2D layer, hindering carrier transfer. Therefore, we add an IPA wash, which can effectively dissolve both the organic ligands and the 2D perovskite,[27,34] to remove excess organic ligands and control the 2D perovskite phase and thickness. Notably, although we chose IPA as the polishing solvent here, any solvent that can dissolve both the organic ligands and 2D perovskite without effectively damaging the 3D perovskite surface should also be a good candidate for this treatment.[35–38] As a result, we remove excess precursors and obtain a phase-pure $n = 2$, 2D perovskite layer, as shown in the GIWAXS graph in Figure 1e, and the net balanced reaction in Equation (2) can be achieved.

$$n\left(PbX_2\right) + (n-1)\,AX + 2\,(LX) \rightarrow L_2A_{n-1}Pb_nX_{3n+1}\,(n = 2) \quad (2)$$

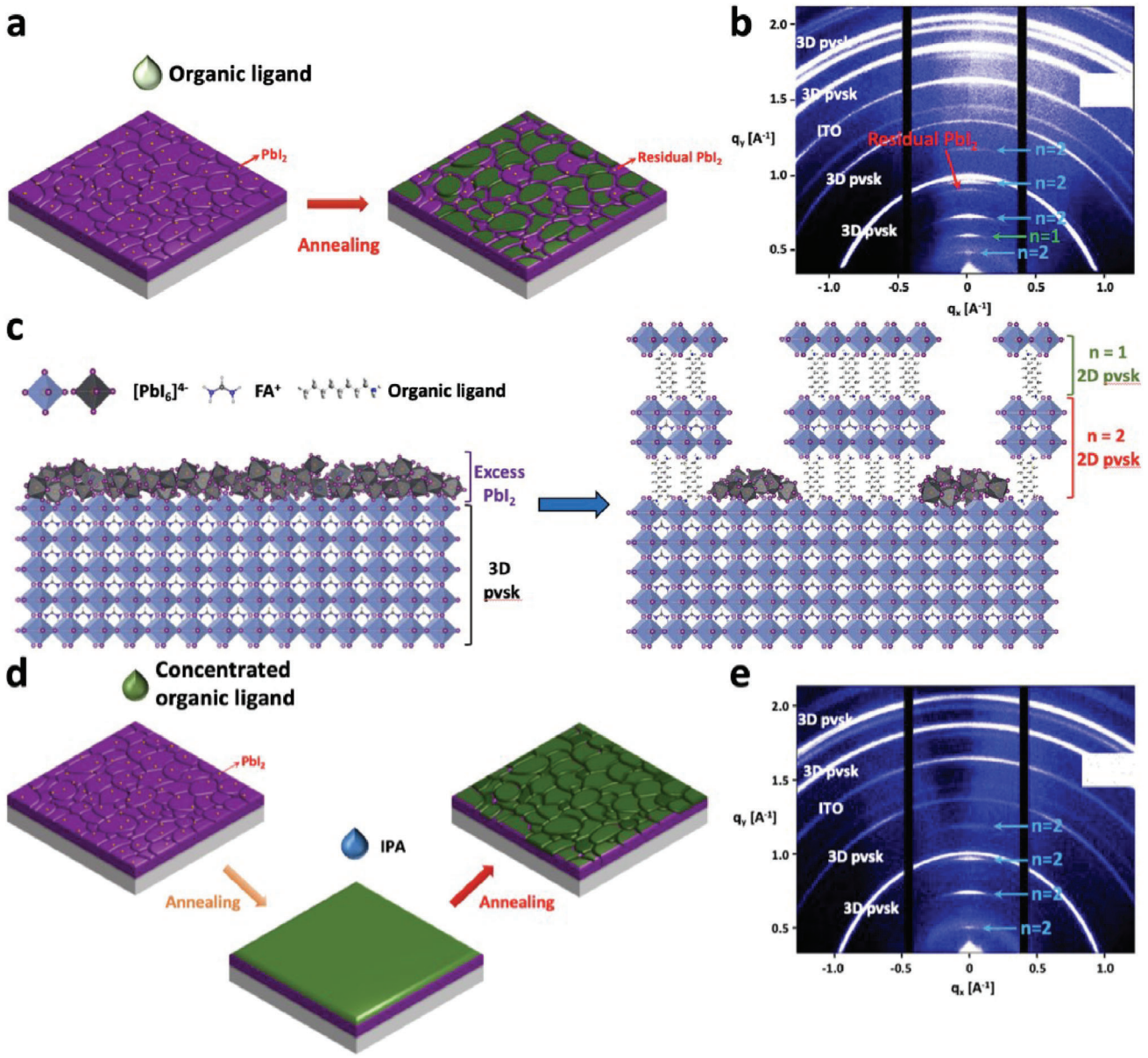

Figure 1. The process and GIWAXS graph of the conventional 2D treatment and our approach. a,b) The procedure and the GIWAXS graph of the conventional 2D treatment. c) The schematic diagram for the conventional 2D treatment. d,e) The procedure and the GIWAX graph of our approach.

3. Effects and Mechanism of Our Approach

In-situ GIWAXS was used to continuously monitor the effect of each step of our approach as shown in **Figure** 2a, and Figure 2b–d show the average GIWAXS graphs of the different stages. Without any treatment, the excess PbI_2, the precursor for 2D perovskite growth, is visible in the GIWAXS graph in Figure 2b. When a concentrated organic ligand solution is introduced to fully consume the excess PbI_2, the PbI_2 peak disappears as indicated in Figure 2a. Then, during the annealing step, the organic ligand gradually reacts and crystallizes with PbI_2 and AX, forming the 2D perovskite. As shown in Figure 2a,c, the $n = 1$ and $n = 2$, 2D perovskite, emerge during the annealing step. Meanwhile, we note that after treatment with an excess of organic ligands, there are residual organic ligands dominantly localized on the surface,[39] and a thick 2D perovskite layer forms on top of the 3D perovskite, with the $n = 1$, 2D perovskite, favorably formed on top, and the $n = 2$, 2D perovskite, buried underneath as illustrated in Figure S1 (Supporting Information) and as reported in the literature.[40] This favorable 2D perovskite growing order may result from the changing stoichiometry of the precursors during the 2D perovskite formation. After treatment with excess organic ligands, the introduced 2D organic ligand first consumes all the dissolved AX from the dissolved perovskite surface and forms the $n = 2$, 2D perovskite, on top of the 3D perovskite. Subsequently, the remaining 2D organic ligands form the 2D perovskite

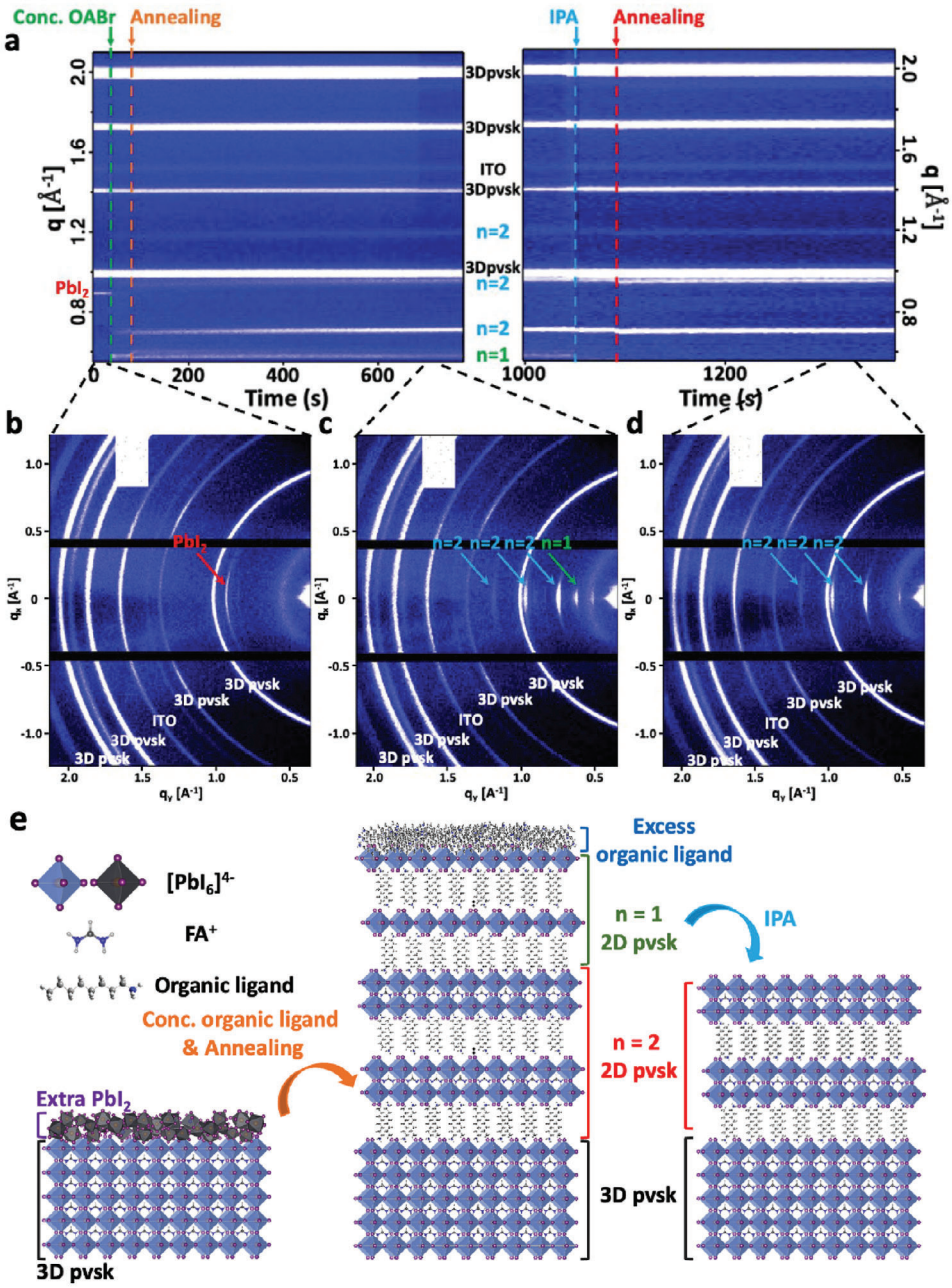

Figure 2. The effects and proposed mechanism of our approach. a) In situ GIWAXS graphs for the method. The two spectra are collected from the same film with separate measurements due to the limited one-time solvent dropping in one measurement. The "conc." is the abbreviation of "concentrated." b–d) The average GIWAXS graphs of the marking time frames. The white rectangles inside the graphs are dead areas on the area detector used for these measurements. e) The schematic diagram for the proposed mechanism of the method.

without an AX source, which forms the $n = 1$, 2D perovskite atop the $n = 2$, 2D perovskite.

To remove the excess organic ligands and control the 2D perovskite phase and thickness, we apply a dynamic IPA wash since IPA can effectively dissolve both organic ligands and 2D perovskite. As indicated in Figure 2a,d, the $n = 1$, 2D perovskite, disappears after the IPA treatment, resulting in a phase-pure, $n = 2$, 2D perovskite. This is because the IPA treatment predominantly dissolves the top surface and the $n = 1$, 2D perovskite, preferably forms on top. Therefore, the IPA treatment removes residual organic ligands, the $n = 1$, 2D perovskite, and some of the underlying $n = 2$, 2D perovskite. Moreover, we can control the 2D perovskite thickness with the annealing step coupled with the IPA treatment. As shown in the X-ray diffraction (XRD) spectra (Figure S3, Supporting Information), the 2D perovskite integrated peak area of the treated films becomes larger if we anneal the 2D perovskite films at higher temperatures or for a longer time before the IPA treatment, inferring different 2D perovskite

film thicknesses after treatment. We assume this is because the 2D perovskite crystalizes from the bottom to the top during the annealing. This implies that we can control the annealing condition, making the top part of 2D perovskite less crystalline and easier to remove with IPA than the bottom layer. Therefore, the controlled annealing condition together with the IPA treatment can then be utilized to tune the 2D thickness (Figure S3, Supporting Information).

We also note that during the IPA treatment, the top layers of thick 2D perovskite (i.e., the extra organic ligands, the upper $n = 1$, 2D perovskite, and some of the $n = 2$, 2D perovskite) are not only eliminated but could also serve as protective layers, preventing the bottom layers, the $n = 2$, 2D perovskite, and the 3D perovskite, from being damaged by the IPA. After the IPA treatment, we again anneal the film to increase the crystallinity of the 2D perovskite. Figure 2e shows the schematic summary of the proposed mechanism. Therefore, with our approach, we obtain a pristine surface (without excess precursors) and with a controlled thickness phase-pure, $n = 2$, 2D perovskite. In addition, we also show that our method is valid for organic ligands with a different halide anion and organic cation, showing its wider generality (Figure S4, Supporting Information).

4. Surface Characteristics

The surface morphology was probed using scanning electron microscopy (SEM), collecting plane-view images of each stage of our approach and conventional 2D solution process as shown in **Figure 3**a. Hereafter, our approach treatment films and devices are marked as "target," and the conventional 2D treatment films and devices are marked as "control." Without any treatment, the bare 3D perovskite films show an abundance of excess PbI_2 (white crystals) on top of the 3D perovskite. After the conventional 2D approach, although some PbI_2 is reacted, we can still observe residual PbI_2 in the control SEM image. In contrast, after our approach, the white crystals (PbI_2) disappear, implying a full reaction and removal of the PbI_2 in the target. The SEM images also clearly demonstrate the cleaning effect of the IPA treatment. Before the IPA treatment, the thick 2D perovskite and excess organic ligands cover the 3D perovskite, blurring the SEM image. Conversely, after the IPA treatment, IPA removes both the excess 2D perovskite and organic ligands, revealing the underlying 3D and 2D perovskite layers. Notably, the surface with the IPA treatment shows no obvious morphology difference from the control, suggesting that the formed thick 2D layer protects the bottom layers from damage from the IPA. Atomic force microscopy (AFM) images in Figure S5 (Supporting Information) also show similar surface topography and height distribution between the target and control, consistent with the SEM images.

Ultraviolet photon spectroscopy (UPS) was conducted to investigate the band alignment of the 3D perovskite and the hole transport layer (HTL), Spiro-MeOTAD, as shown in Figure 3b,c. The impure 2D phase, $n = 1$ and $n = 2$, from the control results in a type I band alignment between the 3D perovskite and HTL. This type I alignment forms an electronic barrier that hinders the extraction of holes from the 3D perovskite to the HTL, consequently increasing the series resistance of the PSCs. On the other hand, the pure, $n = 2$, 2D phase from the target results in a type II band alignment between the 3D perovskite and HTL. This favorable type II alignment creates an energetic cascade between the 3D perovskite and HTL, facilitating the transfer of holes through the interface.

Moreover, we compared the contact angle measurement with water for both treatments to understand the surface hydrophobicity. As shown in Figure S6 (Supporting Information), the average contact angle with water increased from 72.16 °(control) to 83.78 °(target). The increase in the contact angle reflects a more hydrophobic surface for the target, which may be due to a more thorough surface 2D perovskite passivation because of the complete reaction of PbI_2 to the 2D perovskite. This more hydrophobic surface can potentially enhance the stability of PSCs relative to humidity.

5. Charge Carrier Dynamics and Device Performance

Transient reflection spectroscopy (TRS) was utilized to investigate carrier diffusion as a function of depth from the surface (**Figure 4**a).[43] As shown in the fitting result of TRS in Figure 4b, the target surface diffusion coefficient increased by ≈250% compared to the control, while the bulk diffusion coefficient remained the same as the control, indicating that the 2D perovskite grown by our method can effectively passivate the surface without damaging the bulk 3D perovskite. Moreover, time-resolved photoluminescence (TRPL) and time-resolved microwave conductivity (TRMC) spectroscopy were also conducted to investigate surface passivation effects. As illustrated in the TRPL measurements (Figure 4c), the target films show a 47% increase in carrier lifetime from 5.8 µs (control) to 8.5 µs, indicating our approach can effectively reduce defect-assisted non-radiative recombination. In contrast, with TRMC (Figure S7, Supporting Information), a bulk measurement without surface sensitivity, the carrier lifetime of the target increased merely by 5% from 15.0 µs (control) to 15.8 µs. The TRPL coupled with the TRMC results reveal that our approach mainly influences the surface while the bulk 3D perovskite remains largely untouched, consistent with the TRS results.

Figure 4d and Figure S8 (Supporting Information) present the statistical PCEs and corresponding photovoltaic parameters for both the control and target with an FTO/SnO_2/3D/2D/Spiro-OMeTAD/gold structure. As shown in Figure S8 (Supporting Information), the PCE improvement of the target results from the increase of open-circuit voltage (*Voc*) and *FF*; the short-circuit current (*Jsc*) shows a similar average value for these two methods because the perovskite bandgap of the cells stays the same after these two treatments (Figure S9, Supporting Information). The *Jsc* results also match the EQE measurement in Figure S10 (Supporting Information). The increase in *Voc* reflects the lower non-radiative recombination inside the device compared with the control, consistent with the long carrier lifetime we observed in TRPL measurement. On the other hand, the increase in *FF* reflects the low series resistance of the device, which can be ascribed to a better type II energy band alignment owing to the obtained phase-pure, $n = 2$, 2D perovskite and the pristine surface after the treatment. Therefore, PSCs with our approach improved the average PCE from 23.9% to 24.8% and the champion device

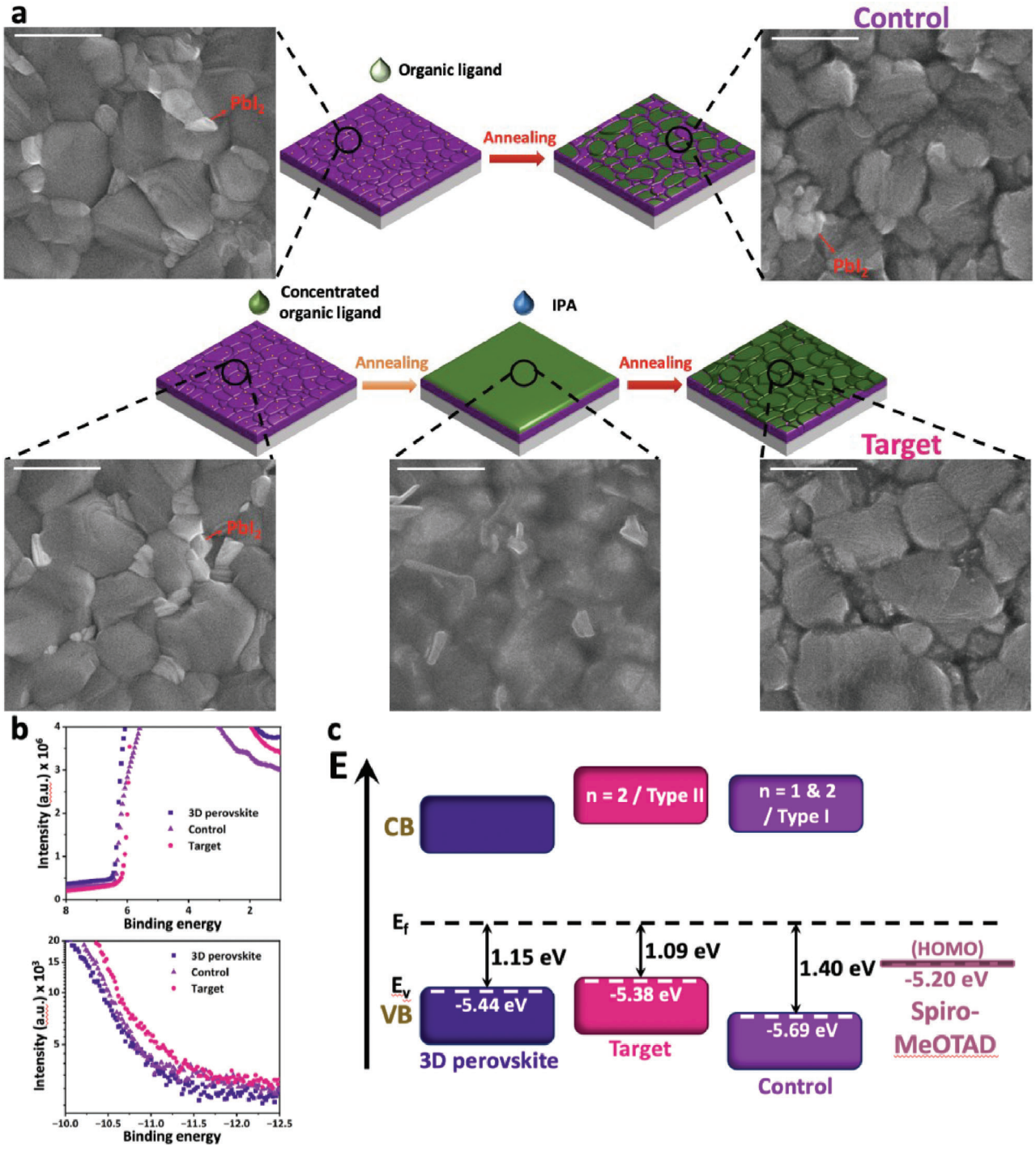

Figure 3. The surface morphology and band diagram of our approach (target) and conventional 2D treatment (control). a) Film surface SEM images correspond to each process step for control and target. The scale bar in the graph represents 1 µm. b) UPS secondary electron cut-offs (top) and valence band spectra (bottom) of the 3D perovskite, control, and target. c) Band alignments between the 3D perovskite, 2D perovskite of control and target films, and the HTL (Spiro-MeOTAD).[41,42]

reached a PCE of 25.3%. Devices made with our approach also show negligible hysteresis (Figure 4e).

Figure 4f shows the stability results of the devices under MPP tracking and continuous 1-sun illumination at ≈40 °C. For the device stability test, oxalic acid chemical bath deposition was used to prepare the electron transporting layer (SnO_2) of the device to enhance the device stability.[44] The regular structure PSC based on our approach retains 80% of the initial PCE after 1270 h, while the control maintains 80% of the initial PCE after 420 h. We attribute the stability enhancement of the PSCs after our approach

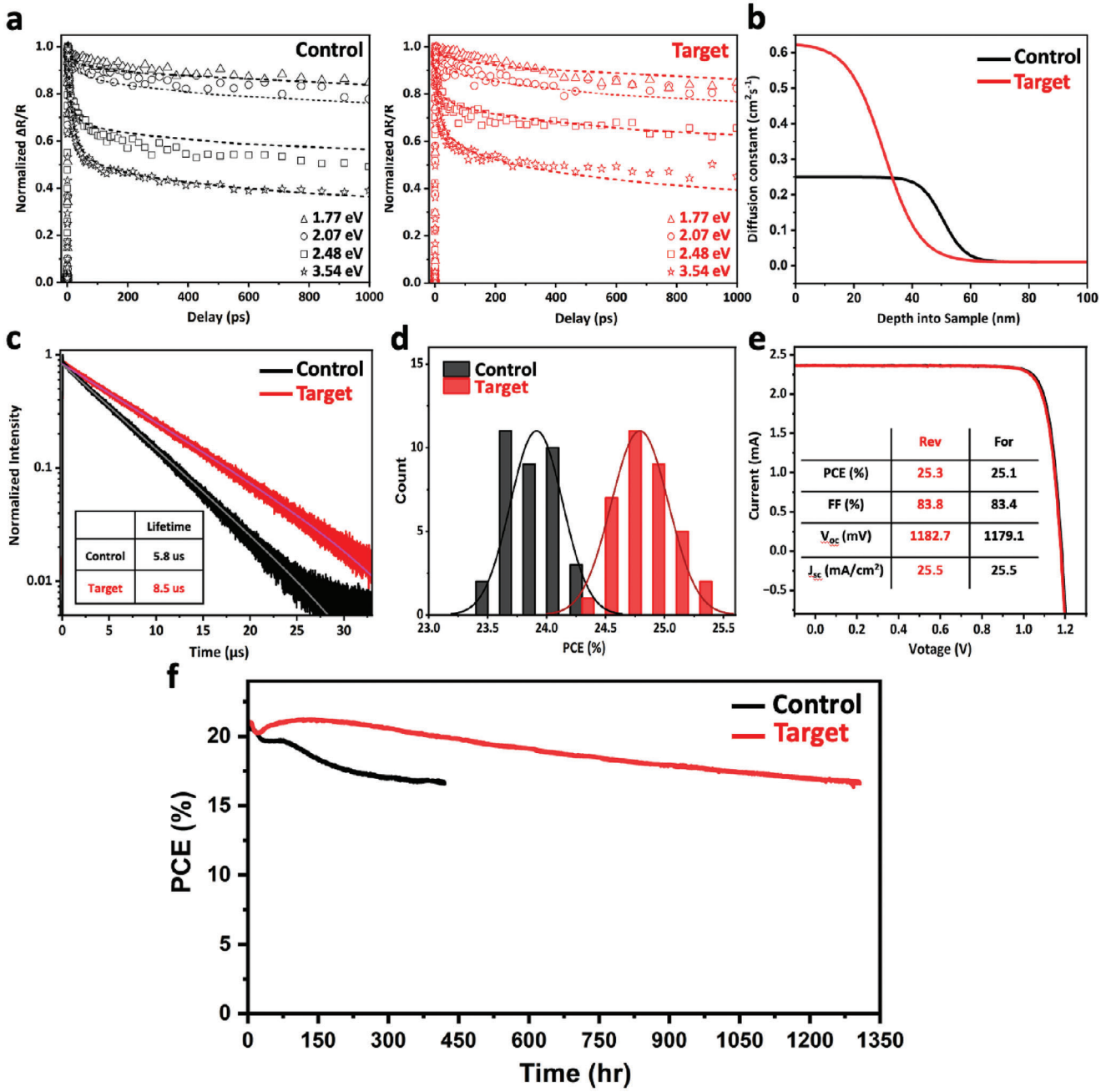

Figure 4. Charge carrier dynamics and device performance. a,b) The TRS spectra and the fitting result. c) The TRPL spectra. d) Device PCE statistic plot. e) The reverse (Rev) and forward (For) scan of the champion device from our method. f) The device stability test of control (PCE at $t = 0$ is 20.7%) and target (PCE at $t = 0$ is 21.1%) under continuous 1-sun illumination and MPP tracking.

to two reasons. First, after the treatment, the residual PbI_2, which is detrimental to the device's stability, can be effectively removed as illustrated by the GIWAXS graph (Figure 2d) and the SEM image (Figure 3a). Second, the favorable type II band alignment and better passivation of the treatment facilitate faster carrier transfer as shown in UPS (Figure 3b,c) and TRS (Figure 4b) data, which can prevent charge accumulation at the interface. Therefore, the method leads to better PSC stability compared to the conventional 2D treatment.

6. Conclusion

We successfully achieved a pristine (without residual 2D precursors) and phase-pure 2D/3D perovskite heterostructure. The consequent $n = 2$, 2D perovskite layer, leads to a favorable type II band alignment between the perovskite and HTL layers, facilitating hole transfer from the 3D perovskite to the HTL. In addition, the formed 2D/3D junction displays an enhanced interface passivation, with a 250% increase in the carrier surface diffusion

coefficient, and a 47% increase in carrier lifetime compared to the control. The resulting PSCs also show a notable improvement in both operational stability and PCE compared to the control, with negligible hysteresis. We anticipate that our approach and design principles will offer valuable insights to enhance interface properties and improve PSC performance.

7. Experimental Section

Sample Preparation: The details of the sample preparation are described in the Supporting Information.

Characterization: The details of all the measurements and the necessary theories are described in the Supporting Information.

Supporting Information

Supporting Information is available from the Wiley Online Library or from the author.

Acknowledgements

M.-C.S., Y.L., and R.Z. were funded by the U.S. Department of Energy, Solar Energy Technologies Office, under award no. DE-EE0009512. S.T. and Y.-K.L. were funded by the U.S. Department of Energy, Solar Energy Technologies Office, under award no. DE-EE0010503. M.J.G. was supported by First Solar, Inc. T.S. and H.Z. were funded by the U.S. Department of Energy, Office of Basic Energy Sciences, Materials Sciences and Engineering Division, Physical Behavior of Materials, under award number DE-SC0021650. T.S. was also funded by a postgraduate fellowship from the Natural Sciences and Engineering Research Council of Canada (NSERC). T.K. acknowledges support by the U.S. Department of Energy (DOE), Office of Science, Office of Basic Energy Sciences, Materials Sciences and Engineering Division under Contract No. DE-AC02-05-CH11231 (D2S2 program KCD2S2). Work at the Advanced Light Source (ALS) was done at beamline 12.3.2 with support by Nobumichi Tamura. The ALS is a DOE Office of Science User Facility under contract no. DE-AC02-05CH11231. Beamtime studies were carried out with support from the Molecular Foundry, a user facility supported by the Office of Science, Office of Basic Energy Sciences, of the U.S. Department of Energy under Contract No. DE-AC02-05CH11231. The work was authored in part by the National Renewable Energy Laboratory, operated by Alliance for Sustainable Energy, LLC, for the U.S. Department of Energy (DOE) under contract no. DE-AC36-08GO28308. TR, TA, and TRMC spectroscopy studies were provided by the Center for Hybrid Organic-Inorganic Semiconductors for Energy (CHOISE), an Energy Frontier Research Center funded by the Office of Basic Energy Sciences, Office of Science within the U.S. Department of Energy.

Open access funding enabled and organized by MIT Hybrid 2025.

Conflict of Interest

The authors declare no conflict of interest.

Author Contributions

M.-C.S., S.T., and Y.L. contributed equally to this work. M.-C.S. developed the idea with continuous discussions with S.T., supervised by M.G.B. M.-C.S., S.T., and Y.L. designed most of the experiments. M.-C.S., S.T., and Y.L. performed the GIWAXS measurements. M.-C.S. and Y.L. conducted the TRPL, SEM, UPS, and contact angle measurements. M.-C.S. conducted the solar cell fabrication and operated the *J–V* characterization and the MPP tracking of the solar cell device. M.-C.S. conducted the AFM and XRD measurements. T.K. and D.-K.L. assisted with the GIWAXS measurements and analyses, supervised by C.M.S.-F. Y.D. performed the TA and TR measurements, supervised by M.C.B. and K.Z. M.C.B. analyzed and developed the model for the TA and TR results. B.W.L. and S.P. performed the TRMC measurements and analyses, supervised by K.Z. T.S. assisted in the optical alignment of the TRPL setup. M.J.G., R.Z., H.Z., and Y.-K.L. provided helpful discussions. M.-C.S., S.T., and M.G.B. wrote the first manuscript draft. All authors contributed feedback and commented on the manuscript.

Data Availability Statement

The data that support the findings of this study are available from the corresponding author upon reasonable request.

Keywords

2D perovskite, interface, passivation, perovskite solar cell, phase pure

Received: October 30, 2024
Revised: February 12, 2025
Published online: March 18, 2025

[1] NREL, Best Research-Cell Efficiency Chart, https://www.nrel.gov/pv/interactive-cell-efficiency.html (accessed: September 2024).
[2] J. J. Yoo, G. Seo, M. R. Chua, T. G. Park, Y. Lu, F. Rotermund, Y.-K. Kim, C. S. Moon, N. J. Jeon, J.-P. Correa-Baena, V. Bulović, S. S. Shin, M. G. Bawendi, J. Seo, *Nature* **2021**, *590*, 587.
[3] Y. Zhao, F. Ma, Z. Qu, S. Yu, T. Shen, H.-X. Deng, X. Chu, X. Peng, Y. Yuan, X. Zhang, J. You, *Science* **2022**, *377*, 531.
[4] J. Park, J. Kim, H.-S. Yun, M. J. Paik, E. Noh, H. J. Mun, M. G. Kim, T. J. Shin, S. I. Seok, *Nature* **2023**, *616*, 724.
[5] H. Chen, C. Liu, J. Xu, A. Maxwell, W. Zhou, Y. Yang, Q. Zhou, A. S. R. Bati, H. Wan, Z. Wang, L. Zeng, J. Wang, P. Serles, Y. Liu, S. Teale, Y. Liu, M. I. Saidaminov, M. Li, N. Rolston, S. Hoogland, T. Filleter, M. G. Kanatzidis, B. Chen, Z. Ning, E. H. Sargent, *Science* **2024**, *384*, 189.
[6] A. H. Proppe, A. Johnston, S. Teale, A. Mahata, R. Quintero-Bermudez, E. H. Jung, L. Grater, T. Cui, T. Filleter, C.-Y. Kim, S. O. Kelley, F. De Angelis, E. H. Sargent, *Nat. Commun.* **2021**, *12*, 3472.
[7] F. Zhang, S. Y. Park, C. Yao, H. Lu, S. P. Dunfield, C. Xiao, S. Uličná, X. Zhao, L. Du Hill, X. Chen, X. Wang, L. E. Mundt, K. H. Stone, L. T. Schelhas, G. Teeter, S. Parkin, E. L. Ratcliff, Y.-L. Loo, J. J. Berry, M. C. Beard, Y. Yan, B. W. Larson, K. Zhu, *Science* **2022**, *375*, 71.
[8] L. Luo, H. Zeng, Z. Wang, M. Li, S. You, B. Chen, A. Maxwell, Q. An, L. Cui, D. Luo, J. Hu, S. Li, X. Cai, W. Li, L. Li, R. Guo, R. Huang, W. Liang, Z.-H. Lu, L. Mai, Y. Rong, E. H. Sargent, X. Li, *Nat. Energy* **2023**, *8*, 1078.
[9] T. Wang, L. Bi, L. Yang, Z. Zeng, X. Ji, Z. Hu, S.-W. Tsang, H.-L. Yip, Q. Fu, A. K.-Y. Jen, Y. Liu, *J. Am. Chem. Soc.* **2024**, *146*, 7555.
[10] Y. Gao, Z. Song, Q. Fu, Y. Chen, L. Yang, Z. Hu, Y. Chen, Y. Liu, *Adv. Mater.* **2024**, *36*, 2405921.
[11] C. Gong, X. Chen, J. Zeng, H. Wang, H. Li, Q. Qian, C. Zhang, Q. Zhuang, X. Yu, S. Gong, H. Yang, B. Xu, J. Chen, Z. Zang, *Adv. Mater.* **2024**, *36*, 2307422.
[12] H. Chen, S. Teale, B. Chen, Y. Hou, L. Grater, T. Zhu, K. Bertens, S. M. Park, H. R. Atapattu, Y. Gao, M. Wei, A. K. Johnston, Q. Zhou, K. Xu, D. Yu, C. Han, T. Cui, E. H. Jung, C. Zhou, W. Zhou, A. H. Proppe, S. Hoogland, F. Laquai, T. Filleter, K. R. Graham, Z. Ning, E. H. Sargent, *Nat. Photonics* **2022**, *16*, 352.
[13] R. He, Z. Yi, Y. Luo, J. Luo, Q. Wei, H. Lai, H. Huang, B. Zou, G. Cui, W. Wang, C. Xiao, S. Ren, C. Chen, C. Wang, G. Xing, F. Fu, D. Zhao, *Adv. Sci.* **2022**, *9*, 2203210.

[14] X. Zhao, T. Liu, Y.-L. Loo, *Adv. Mater.* **2022**, *34*, 2105849.
[15] K. Ma, J. Sun, H. R. Atapattu, B. W. Larson, H. Yang, D. Sun, K. Chen, K. Wang, Y. Lee, Y. Tang, A. Bhoopalam, L. Huang, K. R. Graham, J. Mei, L. Dou, *Sci. Adv.* **2023**, *9*, adg0032.
[16] A. H. Proppe, R. Quintero-Bermudez, H. Tan, O. Voznyy, S. O. Kelley, E. H. Sargent, *J. Am. Chem. Soc.* **2018**, *140*, 2890.
[17] J. Hu, I. W. H. Oswald, S. J. Stuard, M. M. Nahid, N. Zhou, O. F. Williams, Z. Guo, L. Yan, H. Hu, Z. Chen, X. Xiao, Y. Lin, Z. Yang, J. Huang, A. M. Moran, H. Ade, J. R. Neilson, W. You, *Nat. Commun.* **2019**, *10*, 1276.
[18] Y. Hua, Y. Zhou, D. Hong, S. Wan, X. Hu, D. Xie, Y. Tian, *J. Phys. Chem. Lett.* **2019**, *10*, 7025.
[19] Q. Wang, X. Wang, Z. Yang, N. Zhou, Y. Deng, J. Zhao, X. Xiao, P. Rudd, A. Moran, Y. Yan, J. Huang, *Nat. Commun.* **2019**, *10*, 5633.
[20] T. Kodalle, M. M. Byranvand, M. Goudreau, C. Das, R. Roy, M. Kot, S. Briesenick, M. Zohdi, M. Rai, N. Tamura, J. I. Flege, W. Hempel, C. M. Sutter-Fella, M. Saliba, *Adv. Mater.* **2024**, *36*, 2309154.
[21] X. Zhang, R. Munir, Z. Xu, Y. Liu, H. Tsai, W. Nie, J. Li, T. Niu, D.-M. Smilgies, M. G. Kanatzidis, A. D. Mohite, K. Zhao, A. Amassian, S. F. Liu, *Adv. Mater.* **2018**, *30*, 1707166.
[22] J. Ávila, C. Momblona, P. P. Boix, M. Sessolo, H. J. Bolink, *Joule* **2017**, *1*, 431.
[23] M.-G. La-Placa, L. Gil-Escrig, D. Guo, F. Palazon, T. J. Savenije, M. Sessolo, H. J. Bolink, *ACS Energy Lett.* **2019**, *4*, 2893.
[24] D. Lin, T. Zhang, J. Wang, M. Long, F. Xie, J. Chen, B. Wu, T. Shi, K. Yan, W. Xie, P. Liu, J. Xu, *Nano Energy* **2019**, *59*, 619.
[25] Q. Zhou, B. Liu, X. Shai, Y. Li, P. He, H. Yu, C. Chen, Z.-X. Xu, D. Wei, J. Chen, *Chem. Commun.* **2023**, *59*, 4128.
[26] Y.-W. Jang, S. Lee, K. M. Yeom, K. Jeong, K. Choi, M. Choi, J. H. Noh, *Nat. Energy* **2021**, *6*, 63.
[27] S. Sidhik, Y. Wang, M. D. Siena, R. Asadpour, A. J. Torma, T. Terlier, K. Ho, W. Li, A. B. Puthirath, X. Shuai, A. Agrawal, B. Traore, M. Jones, R. Giridharagopal, P. M. Ajayan, J. Strzalka, D. S. Ginger, C. Katan, M. A. Alam, J. Even, M. G. Kanatzidis, A. D. Mohite, *Science* **2022**, *377*, 1425.
[28] L. Mao, C. C. Stoumpos, M. G. Kanatzidis, *J. Am. Chem. Soc.* **2019**, *141*, 1171.
[29] G. Tumen-Ulzii, C. Qin, D. Klotz, M. R. Leyden, P. Wang, M. Auffray, T. Fujihara, T. Matsushima, J. W. Lee, S. J. Lee, Y. Yang, C. Adachi, *Adv. Mater.* **2020**, *32*, 1905035.
[30] Y. Gao, H. Raza, Z. Zhang, W. Chen, Z. Liu, *Adv. Funct. Mater.* **2023**, *33*, 2215171.
[31] D. W. deQuilettes, J. J. Yoo, R. Brenes, F. U. Kosasih, M. Laitz, B. D. Dou, D. J. Graham, K. Ho, Y. Shi, S. S. Shin, C. Ducati, M. G. Bawendi, V. Bulović, *Nat. Energy* **2024**, *9*, 457.
[32] T. Kodalle, R. F. Moral, L. Scalon, R. Szostak, M. Abdelsamie, P. E. Marchezi, A. F. Nogueira, C. M. Sutter-Fella, *Adv. Energy Mater.* **2023**, *13*, 2201490.
[33] H. Gu, J. Xia, C. Liang, Y. Chen, W. Huang, G. Xing, *Nat. Rev. Mater.* **2023**, *8*, 533.
[34] J. J. Yoo, S. Wieghold, M. C. Sponseller, M. R. Chua, S. N. Bertram, N. T. P. Hartono, J. S. Tresback, E. C. Hansen, J.-P. Correa-Baena, V. Bulović, T. Buonassisi, S. S. Shin, M. G. Bawendi, *Energy Environ. Sci.* **2019**, *12*, 2192.
[35] M. Yuan, H. Ma, Q. Dong, X. Wang, L. Zhang, Y. Yin, Z. Ying, J. Guo, W. Shang, J. Zhang, Y. Shi, *Nano Energy* **2024**, *121*, 109192.
[36] H. Wang, L. Deng, Y. Pan, X. Zhang, X. Li, Y. Wang, Y. Wang, Y. Liu, X. Yue, Z. Shi, C. Li, K. Liu, T. Hu, Z. Liang, C. Tian, J. Wang, A. Yu, X. Zhang, Y. Yang, Y. Zhan, *ACS Appl. Mater. Interfaces* **2023**, *15*, 36447.
[37] Y. Xu, L. Zhai, L. Sun, J. Wang, X. Tan, H. Huang, Y. Wang, G. Yang, K. Jiang, Y. Yang, L. Zhang, Z. 'ao Tan, C. Zou, *Chem. Commun.* **2022**, *58*, 7132.
[38] L. Zhao, Q. Li, C.-H. Hou, S. Li, X. Yang, J. Wu, S. Zhang, Q. Hu, Y. Wang, Y. Zhang, Y. Jiang, S. Jia, J.-J. Shyue, T. P. Russell, Q. Gong, X. Hu, R. Zhu, *J. Am. Chem. Soc.* **2022**, *144*, 1700.
[39] N. Mozaffari, T. Duong, M. M. Shehata, A. D. Bui, H. T. Pham, Y. Yin, Y. O. Mayon, J. Zheng, M. A. Mahmud, G. D. Tabi, G. G. Andersson, L. E. Black, J. Peng, H. Shen, T. P. White, K. Weber, K. R. Catchpole, *Sol. RRL* **2022**, *6*, 2200355.
[40] R. Azmi, E. Ugur, A. Seitkhan, F. Aljamaan, A. S. Subbiah, J. Liu, G. T. Harrison, M. I. Nugraha, M. K. Eswaran, M. Babics, Y. Chen, F. Xu, T. G. Allen, A. ur Rehman, C.-L. Wang, T. D. Anthopoulos, U. Schwingenschlögl, M. D. Bastiani, E. Aydin, S. D. Wolf, *Science* **2022**, *376*, 73.
[41] J. Euvrard, Y. Yan, D. B. Mitzi, *Nat. Rev. Mater.* **2021**, *6*, 531.
[42] J. Peng, F. Kremer, D. Walter, Y. Wu, Y. Ji, J. Xiang, W. Liu, T. Duong, H. Shen, T. Lu, F. Brink, D. Zhong, L. Li, O. Lee Cheong Lem, Y. Liu, K. J. Weber, T. P. White, K. R. Catchpole, *Nature* **2022**, *601*, 573.
[43] Y. Yang, M. Yang, D. T. Moore, Y. Yan, E. M. Miller, K. Zhu, M. C. Beard, *Nat. Energy* **2017**, *2*, 16207.
[44] Y. Lu, M.-C. Shih, S. Tan, M. J. Grotevent, L. Wang, H. Zhu, R. Zhang, J.-H. Lee, J.-W. Lee, V. Bulović, M. G. Bawendi, *Adv. Mater.* **2023**, *35*, 2304168.